Noname manuscript No.
(will be inserted by the editor)

Experimental comparison of blade pitch and speed control strategies for horizontal-axis current turbines

Katherine Van Ness · Craig Hill · Justin Burnett · Alberto Aliseda · Brian Polagye

Received: date / Accepted: date

Abstract The majority of utility-scale horizontal-axis current turbines use either speed or pitch control to maintain a constant power output once the currents exceed a certain threshold: the turbine-specific "rated speed". In this study, we experimentally characterized power performance and turbine loading over a range of blade pitch settings and tip-speed ratios for a three-bladed horizontal-axis turbine. We then implemented a control strategy to maintain power output in time-varying currents using blade pitch control and compare the turbine performance under this control strategy to "overspeed" and "underspeed" control strategies for a fixed pitch turbine. The experiments were conducted with a laboratory-scale 0.45-m diameter turbine in an open channel flume with a 35% blockage ratio. During pitch characterization experiments, inflow velocity was maintained at 0.8 m/s with 4% turbulence intensity. During time-varying inflow experiments, currents varied from 0.7-0.8 m/s over a 20-minute period, while a proportional controller regulated either blade pitch or rotor speed, and we recorded turbine power output and turbine loads. In this velocity range, where turbine performance is independent of Reynolds number,

Funding was provided by the Naval Facilities Engineering Command (NAVFAC) under N00024-10-D-6318 Task Order 0067 and N00024-10-D-6318 Task Order N00024-18-F-8702.

K. Van Ness
University of Washington, Seattle, WA, USA
Tel.: +1-740-644-8426
E-mail: kvanness@uw.edu

C. Hill
University of Minnesota Duluth, Duluth, MN, USA

J. Burnett
University of Washington Applied Physics Laboratory, Seattle, WA, USA

A. Aliseda
University of Washington, Seattle, WA, USA

B. Polagye
University of Washington, Seattle, WA, USA

we demonstrated that pitch control substantially reduced torque requirements relative to underspeed control and turbine loads relative to overspeed control. Additional tests were conducted for underspeed control and pitch control in a Reynolds-dependent regime with time-varying inflow between 0.4-0.5 m/s and 0.5-0.6 m/s. These cases suggest that blade pitch control could provide even greater benefits relative to speed control in small-scale applications.

Keywords blade pitch control · horizontal-axis turbine · laboratory-scale · Reynolds number · speed control · turbine loads

1 Introduction

Cost and reliability remain among the main barriers limiting widespread adoption of riverine, estuarine, or ocean current turbine power generation. In particular, structural loads are significantly greater than for wind turbines with equivalent power output, which contributes to higher costs [1]. Compounded with uncertainties about hydrodynamic loads, this can contribute to structural failure or excessive and expensive safety factors [2]. Consequently, control strategies to mitigate structural loads and reduce cost are of considerable importance [3].

When a variable-speed and/or variable-pitch turbine is operating above the cut-in speed (speed at which the turbine begins to generate power) and below the rated speed, the control objective is to maximize the turbine efficiency (ratio of mechanical shaft power to inflow kinetic power). This operating regime is commonly referred to as “Region II” and shown in Figure 1. Power maximizing is typically achieved by variable speed control that maintains a constant tip-speed ratio corresponding to maximum efficiency. The tip-speed ratio, λ is given by

$$\lambda = \omega R / U_\infty \tag{1}$$

where ω is the rotational speed of the turbine, R is the radius, and U_∞ is the free stream flow upstream of the rotor. However, as inflow velocity exceeds the rated flow speed, the control objective is to maintain a constant power output. This operating regime, commonly referred to as "Region III," is the focus of this study. In Region III, active control to either vary speed or vary blade pitch can decrease turbine efficiency to meet the control objective [4]. While not discussed in this study, turbines that rotate at a constant speed and employ fixed-pitch blades can approximate this behavior passively if designed to achieve a progressive, spanwise stall as currents exceed rated speed and the tip-speed ratio decreases.

Variable speed control strategies are classified as "overspeed" or "underspeed" relative to the rotational speed corresponding to maximum efficiency. Overspeed control involves decreasing generator torque to increase the speed of the rotor, such that λ exceeds its optimal value. Since the thrust coefficient and number of operating cycles increases with λ, the drawback of this strategy

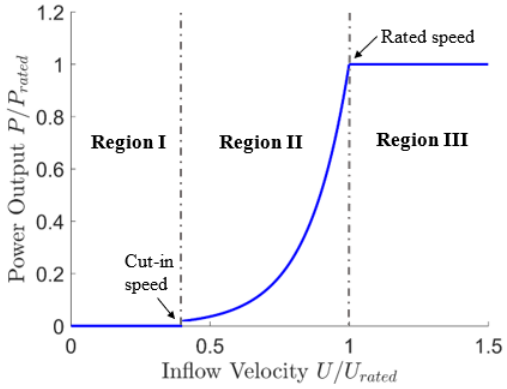

Fig. 1: Canonical power curve for a variable-speed current turbine with operating regimes indicated. Region I corresponds to all current speeds below the cut-in for net generation. Region II corresponds to all current speeds for which the control objective is to maximize power. Region III corresponds to all current speeds for which the control objective is to maintain constant power output.

is that it leads to high fatigue loads and higher material costs for blade manufacturing [4]. Furthermore, depending on the proximity to the water surface, there is also an increased risk of cavitation at high tip-speed ratios, as demonstrated in [5–7]. Underspeed control involves increasing generator torque to decrease the speed of the rotor and bring λ below its optimal value. Lower λ corresponds to lower thrust on the turbine but requires a higher generator torque. This can substantially increase the generator size and, below optimal λ, lift and drag forces can fluctuate rapidly due to blade stall [4]. In comparison, blade pitch control relies on changes in blade pitch to reduce C_P, which can avoid high thrust loads and generator torque. However, installation of pitch actuators introduces additional modes of failure, and inspection, maintenance, and repairs are difficult and expensive for current turbines. Consequently, variable blade pitch mechanisms have not been uniformly adopted by technology developers [8].

To date, blade pitch control performance for current turbines in Region III have been primarily evaluated in simulation [9,10]. While established methods and new demonstrations of pitch control strategies for wind turbines [11, 12] can guide current turbine development, experimental studies using current turbines have been limited to fixed pitch tests for a relatively limited range of blade pitches [7]. Our study compares these control methods experimentally and quantifies the trade-off between variable-pitch and fixed-pitch turbine designs. Further, we explore the implications of control across turbine scale. This can be coarsely partitioned into regimes where characteristic performance varies or is independent of Reynolds number. Most utility-scale turbines will

operate in the Reynolds-independent regime, but laboratory testing or Blue Economy applications [13] involve small rotor dimensions and/or low currents that put them in the Reynolds-dependent regime.

2 Methods

2.1 Scale-model turbine

The laboratory-scale, three-bladed horizontal-axis turbine used for these experiments was 0.45 meters in diameter and designed to allow variable speed and variable pitch. The drive train and instrumentation layout is detailed in Fig. 2. A six-axis load cell (Mini45, ATI Industrial Automation) was installed on the main shaft of the turbine, in the hub, to measure thrust and torque on the rotor. The turbine rotor was connected to a 5:1 gearbox (PV23, Parker Hannifin) and double-shaft stepper motor (LV233, Parker Hannifin), with an optical encoder (ZAA, Applied Motion) mounted on the rear shaft. The stepper motor allowed for precise control of the rotational speed, verified by the encoder measurements. Additional stepper motors (208-13-01D, Lin Engineering), drives (EZHR17EN, All Motion), and optical encoders (E4P, US Digital) were installed in the hub to individually control the pitch angle, β, of each blade in increments of 0.125° via a worm gear and worm wheel. Power and communication signals were transmitted to the rotating hub through a slip ring (SR015 30050-1512-000, Rotary Systems), with the wiring passing through a hollow section of the main shaft. Because load cell measurements are sensitive to temperature, analog temperature sensors (TMP35, Analog Devices) were installed in the nose cone and hub cavity. As the motor was the primary heat source in the nacelle, copper wedges and conductive paste coupled the motor housing to the nacelle wall, increasing conductive heat transfer and minimizing the rise in nacelle air temperature. Further, the hollow section of the main shaft was potted to limit convective heat transfer between the hub and nacelle. Blade geometry, based on the NACA-44 airfoil series, is described in [14].

Data acquisition is shown schematically in Figure 3. The data acquisition script was written using MATLAB and communicated in sequence with the load cell using CAN bus protocol and the stepper motor drives using RS485 protocol. Because of limited space within the hub, we prioritized frame size and torque rating in selecting the blade stepper motors, but the drives had a relatively slow communication rate. Consequently, during steady state inflow tests, when communication with the blade stepper motors was limited to intermittently verifying blade position, the average sampling rate was $\sim$ 100 Hz. However, during the control tests with time-variant inflow, the need for more frequent stepper motor communication decreased the average sampling rate to $\sim$ 35 Hz.

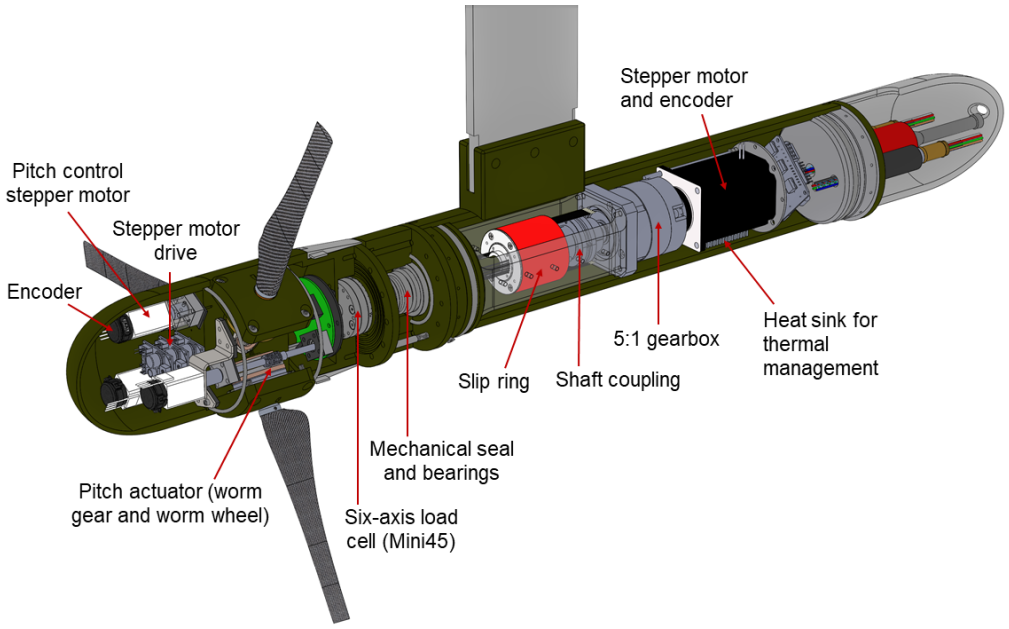

Fig. 2: CAD model of turbine and instrumentation.

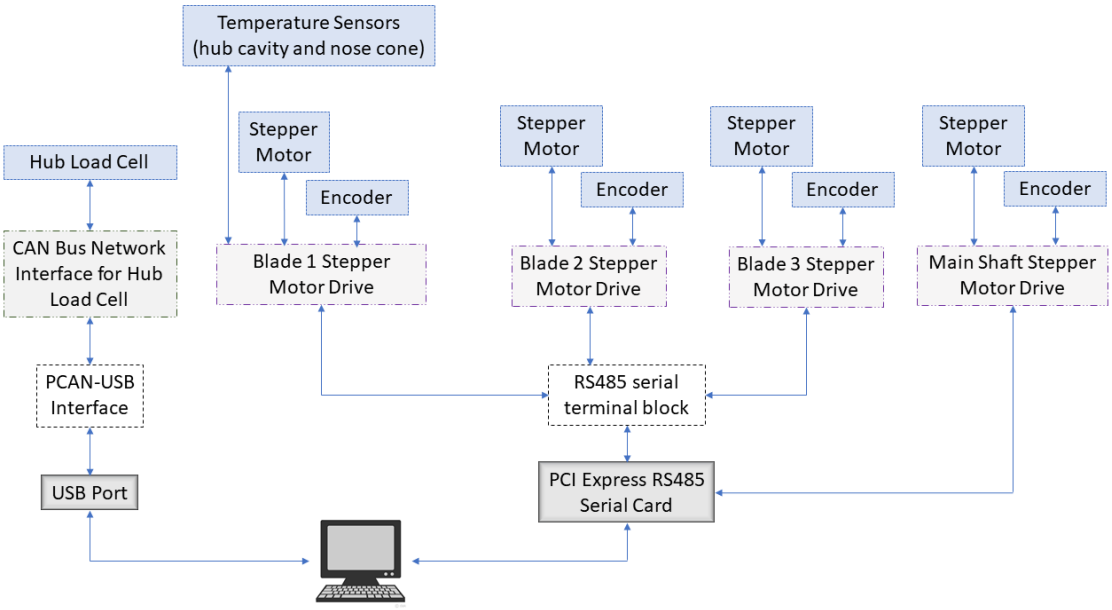

Fig. 3: Data acquisition system block diagram for turbine instrumentation.

Table 1: Turbulence intensities calculated for inflow speeds 0.4-0.8 m/s.

Inflow Speed (m/s)	Mean Turbulence Intensity
0.4	3.2%
0.5	2.2%
0.6	2.0%
0.7	3.4%
0.8	4.4%

2.2 Recirculating open-channel flume

Experiments were conducted in the Alice C. Tyler Flume at the University of Washington, a recirculating open-channel flume with a test section 0.6 meter in depth and 0.76 meter in width. This resulted in a blockage ratio (rotor swept area relative to the channel cross-section) of 35%. Two pumps were controlled by a variable frequency drive to maintain a constant free stream velocity. Depending on the inflow velocity, turbulence intensity, $I = \sqrt{u'^2}/\bar{u}$, ranged from from 2.0% to 4.4% (Table 1), where $\bar{u}$ is the mean inflow velocity and u' is the variation from the mean. The free stream velocity was measured 3 diameters upstream of the rotor plane using an acoustic Doppler velocimeter (ADV, Nortek Vector) sampling at 64 Hz. Chord-based Reynolds number is defined as

$$Re_c = c\sqrt{U_\infty^2 + (\omega r)^2}/\nu, \tag{2}$$

where c is the chord length at 3/4 span (22.8 mm), r is $0.75(D/2)$ (168.75 mm), ν is the kinematic viscosity, and the characteristic velocity scale is an approximate relative velocity that neglects induction. In our experiments, Re_c ranged from $1.3 \cdot 10^4$ at the lowest inflow velocity and tip-speed ratio (0.4 m/s, $\lambda = 1$) to $1.9 \cdot 10^5$ at the highest inflow velocity (0.84 m/s, $\lambda = 10$). Water temperature and, therefore, ν, was maintained by a chiller at $19°C$ for all experiments. Reynolds-independence was observed for $Re_c > 9 \cdot 10^4$, identified when power and thrust coefficients varied by $< 1\%$ when inflow velocity increased from 0.7 m/s to 0.9 m/s and tip-speed ratio and temperature were held constant ($\lambda = 6$, $19°C$). We also note that power and thrust coefficients were within 5% of the Reynolds-independent values for $Re_c > 8 \cdot 10^4$, identified similarly by increasing the inflow velocity from 0.6 to 0.9 m/s while tip-speed ratio and water temperature were held constant.

2.3 Characteristic performance

Prior to control testing, we characterized the turbine performance as a function of blade pitch, β, and tip-speed ratio, λ. For characterization experiments, inflow velocity was maintained at a constant velocity of 0.4, 0.5, 0.6, or 0.8 m/s (see Fig. 4a) to characterize performance in the Reynolds-independent and dependent regimes. Mechanical power output was calculated from the

torque, Q, measured by the six-axis load cell on the driveshaft and rotational speed, ω, from the stepper motor (verified by the optical encoder) and used to compute the coefficient of performance, C_P, in conjunction with the inlet velocity from the ADV as:

$$C_P = \frac{\langle Q\omega \rangle}{0.5\rho A \langle U_\infty^3 \rangle}. \tag{3}$$

where A is the rotor swept area and ρ is the water density. The averages for the mechanical power and kinetic power were calculated separately due to asynchronous clocks. This approximation is reasonable, given the low turbulence intensity in the flume. Thrust, T, measured by the load cell on the driveshaft was used to calculate the coefficient of thrust, C_T, as:

$$C_T = \frac{\langle T \rangle}{0.5\rho A \langle U_\infty^2 \rangle} \tag{4}$$

At each tip-speed ratio, C_P and C_T were calculated over 9000 samples, corresponding to approximately 50-300 revolutions, depending on the rotational speed. Due to blade weight and imperfect weight distribution in the hub, there were azimuthal variations in static force and torque measured by the load cell. To account for this, at the beginning of each test, tare measurements were collected at 12 equidistant azimuthal positions (Fig. 5a). During post-processing, instantaneous force and torque measurements were corrected using a spline interpolation of these values (Fig. 5b).

Performance was characterized for blade pitch angles between $-7°$ and $+33°$ in increments of $5°$ at an inflow velocity of 0.8 m/s (Fig. 6). A positive blade pitch corresponds to a "pitch to feather" strategy (decreasing angle of attack) and negative blade pitch corresponds to a "pitch to stall" strategy (increasing angle of attack). This reference frame is labeled on the schematic in Fig. 7. Note that blade pitch, β, is measured at the blade tip, so a blade pitch of $0°$ indicates that the blade chord line at the tip is parallel to the plane of rotation.

2.4 Region III Control: Reynolds-number independent conditions

First, we consider the case of Region III control when the turbine is operating in a regime where C_P and C_T are independent of Reynolds number. Proportional controllers were used to maintain constant mechanical power by modulating rotational speed or blade pitch (Fig. 8). The "rated" operating condition was defined as the rotational speed corresponding to maximum efficiency for the $-2°$ pitch case at a speed of 0.7 m/s. Pitch control actuated the blade pitch towards feather while holding rotation rate constant. Speed control actuated rotational speed while holding blade pitch constant. Controller gains for speed and pitch control were tuned in an *ad hoc* manner to yield acceptable performance (i.e., rise time, overshoot). This simplistic control was sufficient for our purposes and could be augmented by integral or derivative

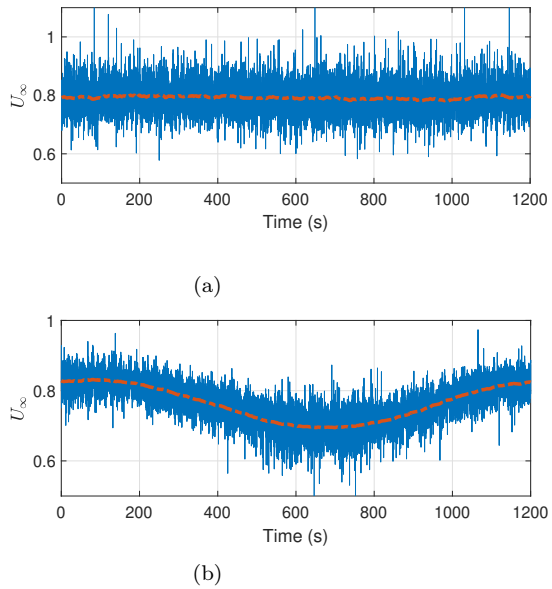

Fig. 4: Representative time series from the ADV during (a) constant inflow averaging 0.8 m/s and (b) oscillating inflow between 0.7 and 0.8 m/s with a 20 minute time period. Orange dashed lines show the one-minute moving average.

gain, or non-linear control [15]. To reduce noise in the input signal to the controller, a moving average filter of 300 samples (20-30 revolutions) was applied to the measured mechanical power. This relatively long averaging window was motivated by the relatively slow data acquisition rate of 35 Hz (limited by the update rate of the blade stepper motors). The controller implementation is shown schematically in Fig. 9. To compare the three control strategies, we oscillated the inflow from 0.7 to 0.8 m/s over a 20-minute period to emulate the low-frequency variation in tidal currents, as shown in Fig. 4b. As shown in Fig. 10, turbine characteristic performance is independent of Reynolds number for most test conditions. However, the underspeed controller, does dip into the Reynolds-dependent regime. The implications of this are discussed further in Sections 4.1 and 4.4. We note that pitch control holds Re_c approximately constant while shedding power, underspeed control reduces Re_c, and overspeed control increases Re_c.

For underspeed and pitch control, controller performance was characterized by the standard deviations of the measured power output relative to the rated power (i.e., control set point). Overspeed control was not implemented experimentally due to physical limitations of the setup. Specifically, at high rotation rates, the main stepper motor produced substantially more heat, causing the nacelle and hub temperatures to rise, which affected load cell accuracy. This was not a concern during the steady state inflow tests, which required only

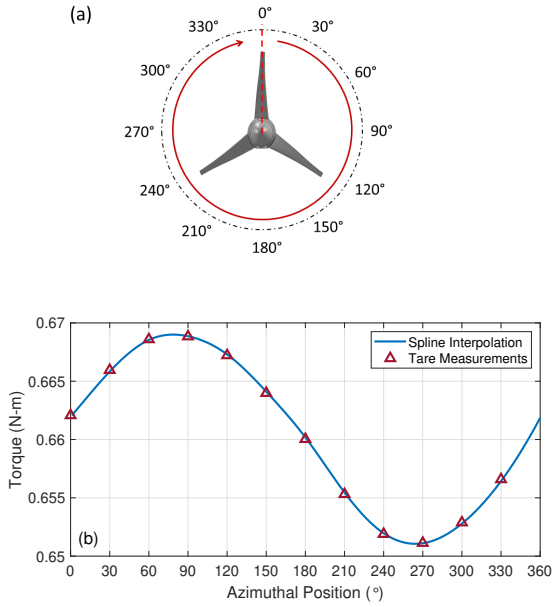

Fig. 5: To account for azimuthally-varying static force and torque, (a) tare measurements were taken at 12 equally-spaced positions and (b) a spline interpolation was used to calculate dynamic loads and torques for instantaneous data.

90-100 seconds of data collection at each tip-speed ratio, such that temperature changes were limited. For this reason, a synthetic overspeed controller was compared to experimental pitch and underspeed controllers. The required efficiency to maintain constant power output was calculated at each point in the experimental inflow time series from the pitch control case and the corresponding thrust and torque values were determined from the performance curves in Fig. 6 for the $-2°$ case. To compare the effects of the controller type on the turbine loads in Region III, mechanical power was normalized by power at the rated operating condition (i.e., P_{rated}), and thrust and torque were similarly normalized by their values at the rated operating condition.

2.5 Region III Control: Reynolds-number dependent conditions

Second, to understand how trends in controller performance change with Reynolds number, we conducted a synthetic experiment using underspeed and pitch control for two Reynolds-number dependent flow regimes: oscillations from 0.4-0.5 m/s and 0.5-0.6 m/s. To do so, we linearly interpolated between the

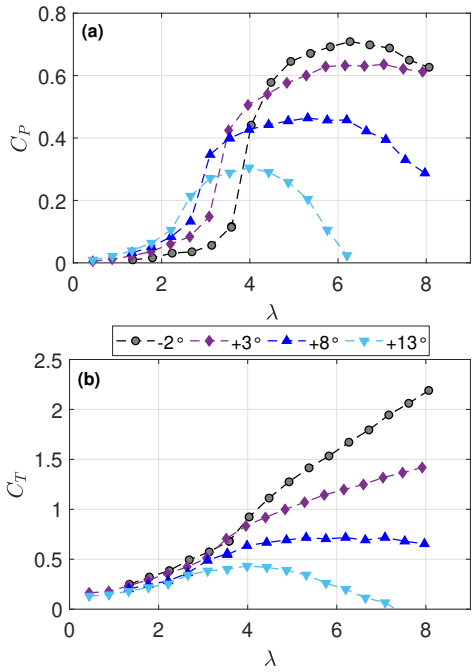

Fig. 6: Coefficients of (a) performance and (b) thrust as a function of tip-speed ratio, λ, for various blade pitch settings at 0.8 m/s inflow velocity. $-2°$ is the optimal pitch angle. Note that the $-2°$ performance curves describe the control space for a fixed-pitch turbine operating with speed control.

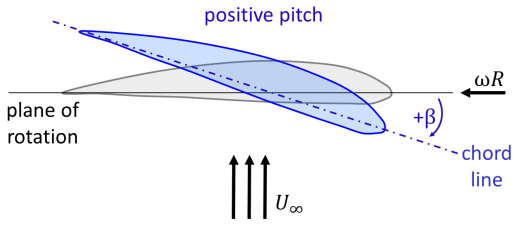

Fig. 7: Blade pitch schematic showing that positive blade pitch angles correspond to blade rotation towards the feathered position (i.e., decreasing the angle of attack). Pitch is measured at the blade tip, so a blade pitch of 0° indicates that the blade chord line at the tip is parallel to the plane of rotation.

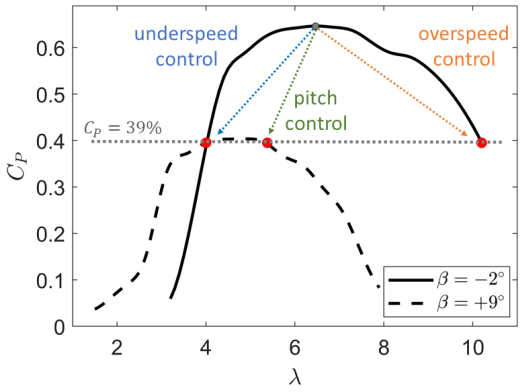

Fig. 8: Underspeed, overspeed, and pitch control can be used to maintain power when inflow oscillates between 0.7 and 0.8 m/s. This requires a 40% reduction in peak efficiency as the inflow speed increases from 0.7 m/s (rated speed) to 0.8 m/s. Underspeed and overspeed control reduce efficiency by increasing or decreasing the tip-speed ratio while blade pitch control involves moving to a separate C_P-λ curve with a lower peak efficiency. Note that the tip-speed ratio changes for pitch control because the inflow velocity changes while rotation rate is held constant.

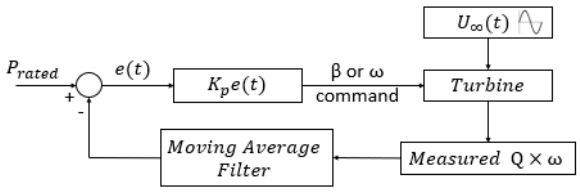

Fig. 9: Proportional controller block diagram.

performance characterizations at constant velocity (included in Appendix A) to obtain C_P and C_T as a function of blade pitch, tip-speed ratio, and inflow velocity and prescribed a sinusoidal inflow velocity. The overspeed cases could not be evaluated in this manner since we could not achieve sufficiently high tip-speed ratios to achieve the required C_P reductions to hold power constant. It is also important to note that, there was a 5° difference in preset pitch angle between the Reynolds-independent control tests and Reynolds-dependent performance characterizations, such that results cannot be directly compared. For this reason, the simulation was repeated for 0.7-0.8 m/s using

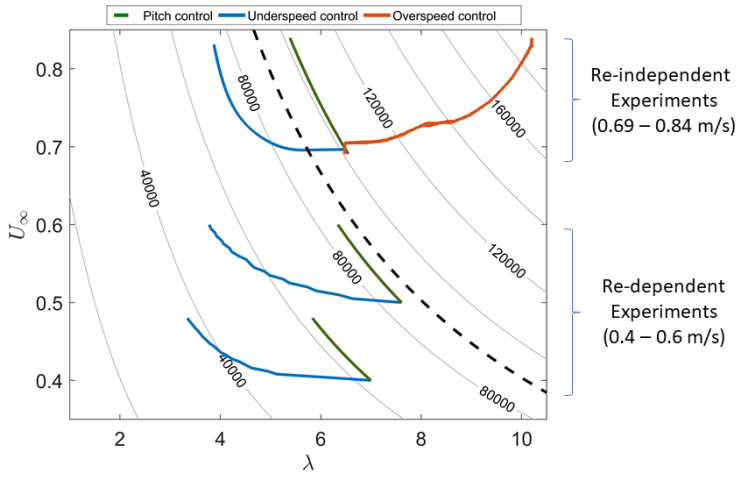

Fig. 10: Contour lines of constant Reynolds number, $Re_c = c\sqrt{U_\infty^2 + (\omega r)^2}/\nu$, as a function of inflow velocity and tip-speed ratio. Lines of constant Re_c are in grey while each colored line corresponds to the range of Reynolds numbers for a particular combination of control strategy and range of inflow velocities. Reynolds-independence was observed above $9 \cdot 10^4$, as denoted by the dashed black line.

the same preset pitch angle to provide comparable results between Reynolds-dependent and Reynolds-independent regimes. This synthetic experiment approach was chosen over physical experiments as a simple matter of expediency. As discussed in Section 3.2, good agreement was observed between experimental results and the synthetic approach. A lower preset pitch angle for the Reynolds-independent tests was necessary to simulate the overspeed controller. At $\beta = 3°$, the peak of the C_P curve was too broad as it extended out to high tip-speed ratios, such that the reduced efficiency required to maintain power could not be achieved within the range of tip-speed ratios tested. At $\beta = -2°$, the C_P curve narrows sufficiently to maintain power within the same tip-speed ratio range, so $\beta = -2°$ was used for these tests. Though the preset pitch angles differ, we can still investigate, separately, the effect of control strategy on turbine loading within each sets of experiments.

3 Results

3.1 Characteristic turbine performance

Figure 6 shows C_P and C_T as a function of tip-speed ratio at an inflow of 0.8 m/s for a subset of blade pitch angles, where -2° is the optimal preset pitch angle. For high tip-speed ratios that are outside the partial stall region (where lift decreases and drag increases), increasing blade pitch towards "feather" (i.e., decreasing the angle of attack) decreases the efficiency and thrust, in line with previously reported experimental results (e.g., [7]). This is reversed for C_P at lower tip-speed ratios, where part of the blade is in stall, as increasing pitch results in reattached flow for part of the blade, producing more lift (i.e., higher efficiency). This result is also in line with previous studies (e.g., [16]).

A contour map of C_P as a function of tip-speed ratio and blade pitch is shown in Fig. 11a. A similar map for C_T is shown in Fig. 11b, while Fig. 11c indicates the operating points where experimental data was collected. We can visualize from the contour maps, interpolated between all pitch characterizations, how we might manipulate β or λ to achieve the efficiency changes required to respond to changing inflow conditions. Furthermore, we can observe the clear limits of overspeed actuation in Fig. 6, looking at the -2° case, which corresponds to the pitch angle for overspeed and underspeed control: C_P decreases slowly as λ increases. Thus, excessive rotation rates would be required to maintain constant power as current speed increases.

Finally, we note that C_P exceeds the Betz limit for some combinations of β or λ. This is simply a consequence of the relatively high blockage ratio under which these experiments were conducted [17, 18].

3.2 Region III Control: Reynolds-number independent regime

Figure 12 shows the time series of oscillating inflow for the pitch control test (with the underspeed test being similar except for the stochastic fluctuations caused by turbulence), calculated power output, controlled speed or pitch, and normalized thrust and torque compared for the three controllers. We again note that the overspeed controller results are synthetic, as this could not be achieved in practice given experimental temperature-control limitations. The implementations of pitch and underspeed control succeeded in maintaining power with a standard deviation of 3-4% for both controllers, which is comparable to the 2% deviation observed during the constant inflow experiments over the same tip-speed ratios and with the same filtering. Controller ability to maintain power can be seen visually in the time series of the oscillating inflow velocity (Fig. 12a) and power output relative to the rated power (Fig. 12c). For comparison, the power output would exceed the rated power by 60 % if no control was employed (i.e., pitch and rotation rate remained constant as inflow velocity increased). The actuated rotational speed or pitch for each control strategy is shown in Fig. 12b.

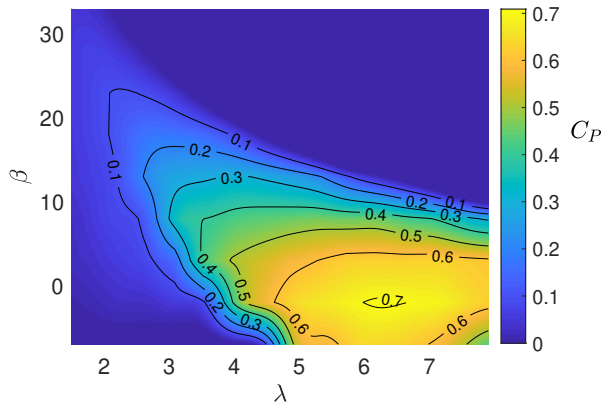

(a)

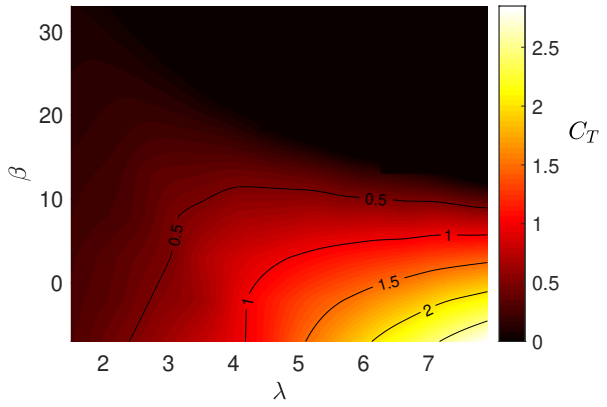

(b)

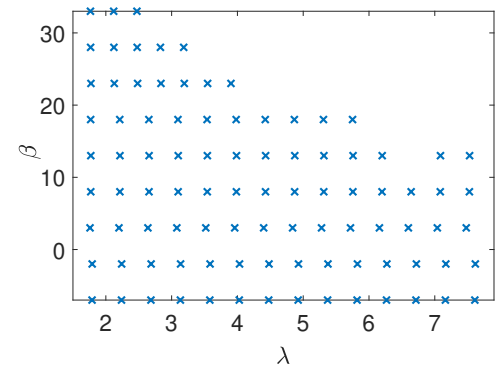

(c)

Fig. 11: (a) C_P and (b) C_T contour maps as a function of tip-speed ratio (λ) and blade pitch (β) in 0.8 m/s flow. (c) indicates operating points where experimental data was collected.

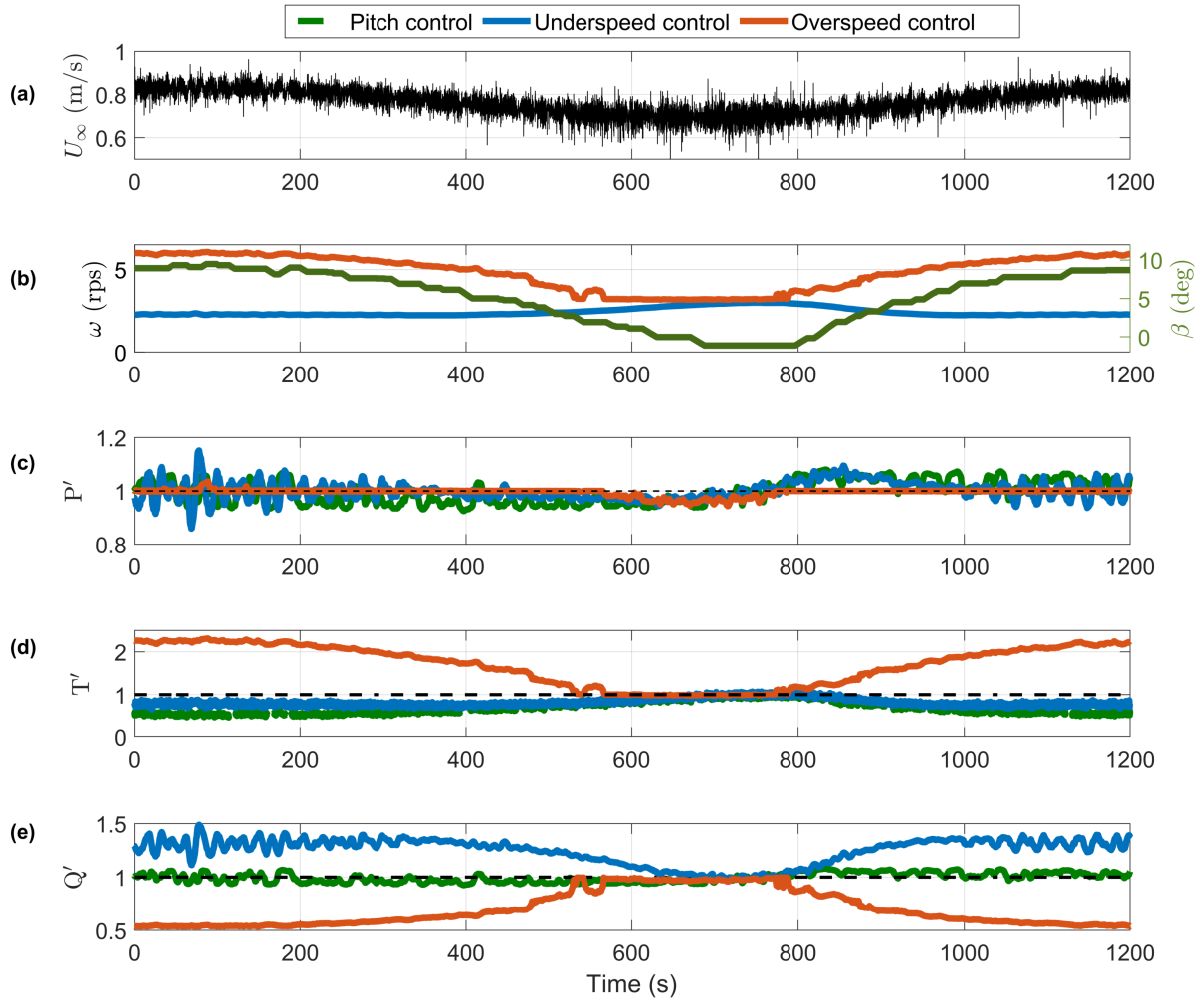

Fig. 12: Time series for (a) free stream velocity, (b) rotor speed (left axis) for speed control or blade pitch (right axis) for pitch control, (c) power output relative to the rated power (d) normalized rotor thrust, and (e) normalized rotor torque for overspeed, underspeed, and pitch control. The overspeed case is a synthetic output based on the measured free stream velocity during the pitch control case and the performance characterization from Fig. 6. For both under- and overspeed control, blade pitch was maintained at $-2°$. For pitch control, rotor speed was maintained at 3.2 rps.

Table 2: Maximum changes in torque and thrust from the rated condition for each controller in 0.7-0.8 m/s oscillating inflow. Blade preset pitch angle is $-2°$.

Controller	Maximum change in torque from rated condition	Maximum change in thrust from rated condition
overspeed (synthetic)	-46%	+127%
underspeed (experimental)	+35%	-25%
pitch (experimental)	+5%	-48%

As expected, we observed that operating in an overspeed mode reduces torque but dramatically increases thrust and vice versa for underspeed control. It should be noted that because of the steep drop-off in efficiency at tip-speed ratios below the rated condition (Fig. 6a), only slight changes in rotational speed were required for underspeed control and, consequently, rotation rate appears almost constant in the time series in Fig. 12b. For the pitch control, since the turbine maintained constant rotational speed and power, torque stayed at its rated value, but as the blades pitched towards feather, rotor thrust was significantly reduced. This is a realization of the characteristic performance shown in Fig. 6, where we see that increasing the pitch at a constant tip-speed ratio decreases C_P and C_T. Because of this, pitch control reduces thrust below the rated condition while maintaining constant power and torque. A summary of the maximum changes in torque and thrust from the rated condition for each control case is provided in Table 2.

To confirm that the synthetic overspeed control performance is realistic, we compared the experimental underspeed controller with a synthetic underspeed controller using the same methodology used for overspeed. The mean change in torque and thrust for the synthetic underspeed controller remained within 2% of the experimental values. Consequently, the synthetic overspeed results are likely a good approximation of what would be observed experimentally and the synthetic approach should be similarly effective in the Reynolds-number dependent regime.

3.3 Region III Control: Reynolds-number dependent regime

Figure 13 and Table 3 show equivalent results for synthetic underspeed and pitch controllers operating in a Reynolds-number dependent regime. For these cases, performance at maximum efficiency for either 0.4 or 0.5 m/s is taken as the "rated" condition. As in the Reynolds-independent regime, we observe comparable thrust loads, with either strategy bringing thrust $20-35$ % below the rated value (Table 3). Again, for pitch control, the torque is constant. Underspeed control, however, increases the maximum normalized torque by 75% in 0.4 – 0.5 m/s flow and 68% in 0.5 – 0.6 m/s flow. For comparison to the Reynolds-independent regime, the synthetic 0.7-0.8 m/s case for underspeed and pitch control is also shown in Fig. 13 and Table 3. Maximum changes

in normalized thrust were, again, similar between controllers and inflow cases while the torque averaged 49% above the rated value for the underspeed controller, a smaller load increase than in the Reynolds-dependent regime. As a reminder, the synthetic 0.7-0.8 m/s results in Table 3 differ from the experimental results in Table 2 because different preset pitch angles were used to define the rated condition.

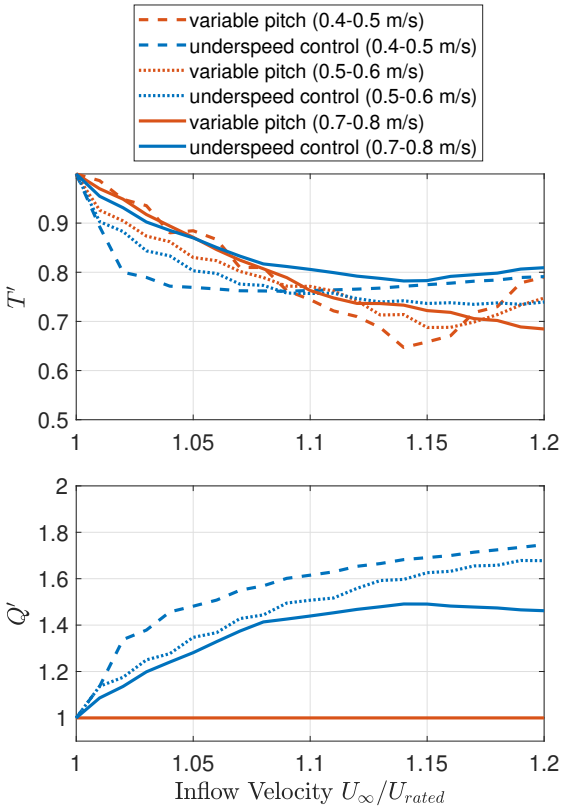

Fig. 13: Normalized (a) rotor thrust and (b) rotor torque using underspeed and pitch control, simulated in oscillating inflow ranges of 0.4-0.5 m/s, 0.5-0.6 m/s, and 0.7-0.8 m/s.

Table 3: Maximum changes in torque and thrust from the rated condition for each controller, simulated for two oscillating inflow cases below Reynolds-independence (0.4-0.5 m/s and 0.5-0.6 m/s) and one case at Reynolds-independence (0.7-0.8 m/s). Blade present pitch angle is +3°.

Inflow Range	Controller	Maximum change in torque from rated condition	Maximum change in thrust from rated condition
0.4-0.5 m/s	Underspeed	+75%	-24%
	Pitch	0%	-35%
0.5-0.6 m/s	Underspeed	+68%	-27%
	Pitch	0%	-31%
0.7-0.8 m/s	Underspeed	+49%	-22%
	Pitch	0%	-32%

4 Discussion

4.1 Reynolds number effects

In lower flow speeds, turbine performance and hydrodynamic loading are a function of tip-speed ratio, blade pitch, and Reynolds number, so relative changes in thrust and torque with blade pitch or rotational speed are accentuated. For example, a turbine using overspeed control in a Reynolds-independent regime sees an increase in kinetic energy available at higher flow speeds and must increase rotational speed to decrease efficiency and maintain power; however, a turbine using overspeed control in a Reynolds-dependent regime sees both an increase in kinetic energy and an increase in C_P and C_T at higher Reynolds numbers, so the required rotational speed to maintain power must counteract both. These excessive rotational speeds result in exacerbated thrust loads relative to overspeed control in Reynolds-independent regimes.

This means that the advantages and disadvantages of each controller are exaggerated below Reynolds-independence. This increases the relative benefit of pitch control, which can accommodate variations in current in Region III without increasing torque or thrust. For example, in Fig. 13 and Table 3, we see that while reductions in normalized thrust for the blade pitch and underspeed controllers are comparable for all three inflow ranges, the normalized torque increases consistently for underspeed control as we move further into the Reynolds-dependent regime. Practically, this would increase generator unit costs for underspeed control relative to blade pitch control.

The distinction between Reynolds-independent and Reynolds-dependent experiments presented in this study is imperfect, as the underspeed controller dips below the threshold for Reynolds-independence at inflow speeds that result in Reynolds independence for the other two controllers. Because load reductions/increases for each controller are exaggerated below Reynolds-independence, it is likely that the underspeed controller produces a slightly

higher torque and lower thrust in experiments (Table 2) than if the inflow velocity was high enough to achieve Reynolds independence for all three controllers. However, power and thrust coefficients within 5% of the Reynolds-independent values occurred above $8 \cdot 10^4$, such that consequences of Reynolds dependence are likely limited. Furthermore, the synthetic pitch controller tested in 0.5-0.6 m/s inflow operates nearly at Reynolds-independence (Fig. 10) and, consequently, there is almost no difference in maximum thrust between the 0.5-0.6 m/s and 0.7-0.8 m/s pitch controllers reported in Table 3. However, because the underspeed controller remains Reynolds-dependent and the pitch controller always maintains constant torque, this still provides insight into torque reductions relative to underspeed control is as we move further into the Reynolds-dependent regime.

It is important to note that our synthetic evaluation is based on the effects of linear interpolation between a range of constant speed inflow conditions. Curvature between interpolation points is anticipated at lower Reynolds number (Figure 10). This likely means that the simulated loads are underpredicted at lower Reynolds numbers since increases in torque and thrust coefficients with Reynolds number become smaller as C_P and C_T approach Reynolds-independence (Fig. 10). Consequently, thrust loads may be similarly underpredicted for the pitch and underspeed control. However, the relative benefit of blade pitch control is likely even greater than shown in Table 2 due to the underpredicted torque loads compared to the constant torque maintained during blade pitch control.

4.2 Blockage effects

Turbine performance in this study is affected by the relatively high blockage ratio (35%) in the test section. Blockage limits expansion of the streamlines around the turbine, resulting in higher flow velocity through the rotor plane and, thus, higher thrust and power than in an unconfined channel [19]. Because equivalent unconfined performance depends on the blockage ratio and rotor thrust [18, 20] and the rotor thrust varies between and within each control scheme, the absolute differences between control schemes are specific to this operational setting. This is also an important distinction between current turbines, which can operate in confined flows, and wind turbines, which are unconfined. It is likely that the high blockage ratio in these experiments exacerbated the thrust loads at high tip-speed ratios, further broadening the peak in C_P to the disadvantage of overspeed control. This effect is demonstrated in the blockage-corrected results (produced using the model presented in [21]) for a pitch angle of -2° in 0.8 m/s flow (Fig. 14), where we observed a reduction in C_P and C_T over most tip-speed ratios and a narrower peak in C_P. While this does not discount the excessive loading found in overspeed control relative to underspeed and pitch control, similar experiments conducted in unconfined flow would be useful for determining more exact loading estimates.

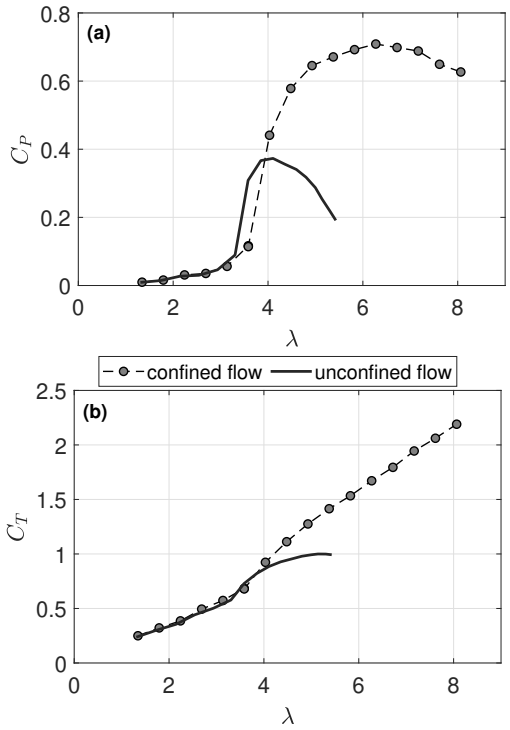

Fig. 14: Coefficients of (a) performance and (b) thrust as a function of tip-speed ratio, λ, for the turbine in confined flow (35% blockage) and unconfined flow. The confined flow result is based on experimental measurements in 0.8 m/s flow with a pitch angle of $-2°$, while the unconfined flow result is estimated using a blockage correction based on the model presented by Houlsby et al. [21].

4.3 Turbulence Effects

The turbulence intensities, I, observed in this study and reported in Table 1 were relatively low (2-4%). Increased turbulence levels generally have negative impacts on turbine performance, including decreased C_P and higher fluctuations in power and thrust [22]. However, at lower Reynolds number, turbulence can improve performance by tripping an early development of a turbulent boundary layer on the blades and prevent the formation of a laminar separation bubble which would otherwise thicken the boundary layer and lead to partial stall and reduced lift.

In this study, at $\lambda = 6$, $U_\infty = 0.6$ m/s, and $I = 2\%$, we were within 5% of Reynolds-independent C_P values, so it is unlikely that the higher turbulence intensities at higher inflow velocities have a significant effect on our experi-

ments. However, advantages of pitch control may be influenced by the higher turbulence intensities at actual tidal energy sites. Specifically, while turbulence intensities may be as low as $5-6\%$ at some sites [2], locations with higher turbulence intensity, such as 10-15% [23, 24], may trip the boundary layer to turbulence and produce Reynolds-independent performance at relatively low Re_c. This would reduce the magnitude of torque and thrust changes reported in Table 3 and the relative advantages of pitch control.

4.4 Choice of Region III controller

We have demonstrated clear advantage for variable blade pitch control in Region III for thrust and torque. We also note, that in the experiments presented here, we increased the water velocity to 15-25% above the turbine's rated speed, while tidal sites may regularly see velocities more than 50% above the rated speed (e.g., [25]). Larger excursions would likely amplify the differences between controllers. However, blade pitch control comes with the cost and complexity of the design and maintenance of pitch control mechanisms. While it is likely less costly than overspeed control, which increases design loads for the blades and support structures, pitch control may be similar in cost to underspeed control which requires only a moderate increase in generator size to accommodate elevated electrical current as a consequence of higher torque. The range of flow speeds a turbine encounters will determine the benefit of pitch control relative to underspeed control. For example, in some river or ocean current environments, relatively limited excursions around rated speed might be anticipated, though flood and drought conditions may still impact design specifications. We also note that industrial accreditation schemes often require turbines to survive control system failures (i.e., pitch or speed control failure resulting in higher than expected thrust, torque, and/or power). Future work should evaluate the implications of control failure modes on design conditions, not just the implications under normal operating conditions.

While this study examined pitch control compared to speed control in low-frequency flow variations and its ability to reduce peak loading, controller performance in high-frequency variations was not examined and may also influence the choice of Region III controller. The potential for pitch controllers to respond to such high-frequency fluctuations (e.g., from turbulence, waves, shear flow, tower shadow) is dependent on frequency, maximum pitch rate and acceleration of the motors, and required power draw, among other design specifications and flow conditions. While pitch control update rate was limited due to hardware selection, a similar study that compares control strategies in response to high-frequency load fluctuations would be valuable in understanding their potential for smoothing blades loads and improving fatigue life.

Another factor in choice of controller is blade geometric profile and the resulting $C_P(\lambda)$ curve. In this study, our specific blade geometry resulted in a broad performance peak, which requires relatively high tip-speed ratios to maintain constant power with overspeed control. The exact load reduc-

tions/increases for a speed/pitch controller will depend on the blade geometry and corresponding performance curves. In applications with a narrow peak in C_P, the observed thrust loads for an overspeed controller may be reasonable enough to consider it a viable option against pitch control. However, broad peaks in C_P reduce the demands for Region II control.

5 Conclusions

While Region III blade pitch control is standard practice in wind turbine design, it is not uniformly employed by current turbines. Experiments were conducted with a scale-model turbine in oscillating inflow to mimic low-frequency fluctuations above the turbine's rated inflow speed. Proportional underspeed and pitch controllers were implemented experimentally, while overspeed control was emulated in a Reynolds-number independent regime. All three control types were then emulated in Reynolds-number dependent regimes.

Results demonstrate that, regardless of Reynolds-number dependence, pitch control significantly reduces the thrust and torque relative to either speed control strategy. Further, the relative benefit from pitch control increases at lower Reynolds number. Ultimately, controller selection requires considering costs and benefits of each control strategy. The higher turbine loads for overspeed control suggest this control strategy may only be viable for current turbines with specific blade geometries and may be particularly poorly suited to turbines operating in confined flow. The choice between pitch and underspeed control may be more subtle, depending on the specifics of turbine design and variation in operating conditions.

Declarations

5.1 Funding

Funding was provided by the Naval Facilities Engineering Command (NAVFAC) under N00024-10-D-6318 Task Order 0067 and N00024-10-D-6318 Task Order N00024-18-F-8702.

5.2 Conflicts of interest/Competing interests

The authors have no competing interests to declare.

5.3 Availability of data and material

The data that supports this work will be available on ResearchWorks, the University of Washington's digital repository.

5.4 Code availability

The code that supports this work will be available on ResearchWorks, the University of Washington's digital repository.

Acknowledgements Experimental facilities at the University of Washington are supported by the Alice C. Tyler Charitable Trust. Additional thanks to Corey Crisp for his ongoing contributions to the laboratory-scale turbine upgrades and to Hannah Ross for providing the blockage correction code used for these results.

References

1. O'Rourke, F., Boyle, F., Reynolds, A. Marine current energy devices: Current status and possible future applications in Ireland. *Renewable and Sustainable Energy Reviews*, 14(3): 1026-1036 (2010).
2. Milne, I.A.; Day, A.H.; Sharma, R.N.; Flay, R.G.L. The characterization of the hydrodynamic loads on tidal turbines due to turbulence. *Renewable and Sustainable Energy Reviews*, 56: 851-864 (2016).
3. Milne, I.A.; Day, A.H.; Sharma, R.N.; Flay, R.G.L. Blade loading on tidal turbines for uniform unsteady flow. *Renewable Energy*, 77: 338-350 (2015).
4. Arnold, M., Biskup, F., Wen Cheng, P. Load reduction potential of variable speed control approaches for fixed pitch tidal turbines. *International Journal of Marine Energy*, 15: 175-190 (2016).
5. Wimshurst, A., Vogel, C., Willden, R. Cavitation limits on tidal turbine performance. *Ocean Engineering*, 152: 223-233 (2018).
6. Kaufmann, N., Carolus, T.H., Starzmann, R. An enhanced and validated performance and cavitation prediction model for horizontal axis tidal turbines.
7. Bahaj, A.S., Molland, A.F., Chaplin, J.R., Batten, W.M.J. Power and thrust measurements of marine current turbines under various hydrodynamic flow conditions in a cavitation tunnel and a towing tank. *Renewable Energy*, 32:407–426 (2007).
8. Zhou, Z., Benbouzid, M., Charpentier, J., Scuiller F. Developments in large marine current turbine technologies - a review. *Renewable and Sustainable Energy Reviews*, 71: 852-858 (2017).
9. Gu, Y., Lin, Y., Xu, Q., Liu, H., Li, W., Blade pitch system for tidal current turbines with reduced variation pitch control strategy based on tidal current velocity preview. *Renewable Energy*, 115:149-158 (2018).
10. Whitby, B. and Ugalde-Loo, C.E. Performance of pitch and stall regulated tidal stream turbines. *IEEE Transaction on Sustainable Energy*, 5:64-72 (2014).
11. Laks, J.H., Pao, L.Y., Wright, A.D. Control of Wind Turbine: Past, Present, Future. *IEEE Xplore* (2009).
12. Bossanyi, E.A., Fleming, P.A., Wright, A.D. Control of Wind Turbine: Past, Present, Future. *IEEE Xplore* (2009).
13. Copping, A., LiVecchi, A., Spence, H., Gorton, A., Jenne, S., Preus, R., Gill, G., Robichaud, R., and Gore, S. Maritime renewable energy markets: Power from the sea. *Maritime Technology Society Journal*, 52(5): 99-109 (2018).
14. R.B. Barber, C.S. Hill, P.F. Babuska, R. Wiebe, A. Aliseda, and M. Motley. Flume-scale testing of an adaptive pitch marine hydrokinertic turbine. *Composite Structures*, 168: 465-473 (2017).
15. D. Forbush, Cavagnaro, R., Polagye, B. Power-tracking control for cross-flow turbines. *Journal of Renewable and Sustainable Energy*, 11 (2019).
16. Gaurier, B., Germain, G., Facq, J.V., Johnstone, C.M., Grant, A.D., Day, A.H., Nixon, E., Di Felice, F., Costanzo, M. Tidal energy "Round Robin" tests comparisons between towing tank and circulating tank results. *International Journal of Marine Energy*, 12:87–109 (2015).

17. Garrett, C., and Cummins, P. The efficiency of a turbine in a tidal channel. *Journal of Fluid Mechanics*, 588: 243-251 (2007).
18. Ross, H. and Polagye, B. An experimental assessment of analytical blockage corrections for turbines. *Renewable Energy*, 152: 1328-1341 (2020).
19. Whelan, J.I., Graham, J.M.R., Peiro, J. A free-surface and blockage correction for tidal turbines. *Journal of Fluid Mechanics*, 624:281-291 (2009).
20. Barnsley, M.J., Wellicome, J.F. Final Report on the 2nd phase of development and testing of a horizontal axis wind turbine test rig for the investigation of stall regulation aerodynamics. Technical report E.5A/CON5103/1746 (1990).
21. Houlsby, G.T., Draper, S., Oldfield, M.L.G. Application of linear momentum actuator disc theory to open channel flow. University of Oxford, Technical Report OUEL 2296/08 (2008).
22. Mycek, P., Gaurier, B., Germain, G., Pinon, G., Rivoalen, E. Experimental study of the turbulence intensity effects on marine current turbines behaviour. Part 1: One single turbine. *Renewable Energy*, 66:729-746 (2014).
23. Gunawan, B., Neary, V.S., Colby, J. Tidal energy site resource assessment in the East River tidal strait, near Roosevelt Island, New York, New York. Renew Energy, 71; 2014. p. 509–17.
24. Thomson, J., Polagye, B., Durgesh, V., Richmond, M. Measurements of Turbulence at Two Tidal Energy Sites in Puget Sound, WA. *IEEE Journal of Oceanic Engineering*, 37(3):363-374 (2012).
25. Lewis, M., McNaughton, J., Marquez-Dominguez, C., Todeschini, G., Togneri, M., Masters, I., Allmark, M., Stallard, T., Neill, S., Goward-Brown, A., Robins, P. Power variability of tidal-stream energy and implications for electricity supply. *Energy*, 183: 1061-1074 (2019).

Appendix A

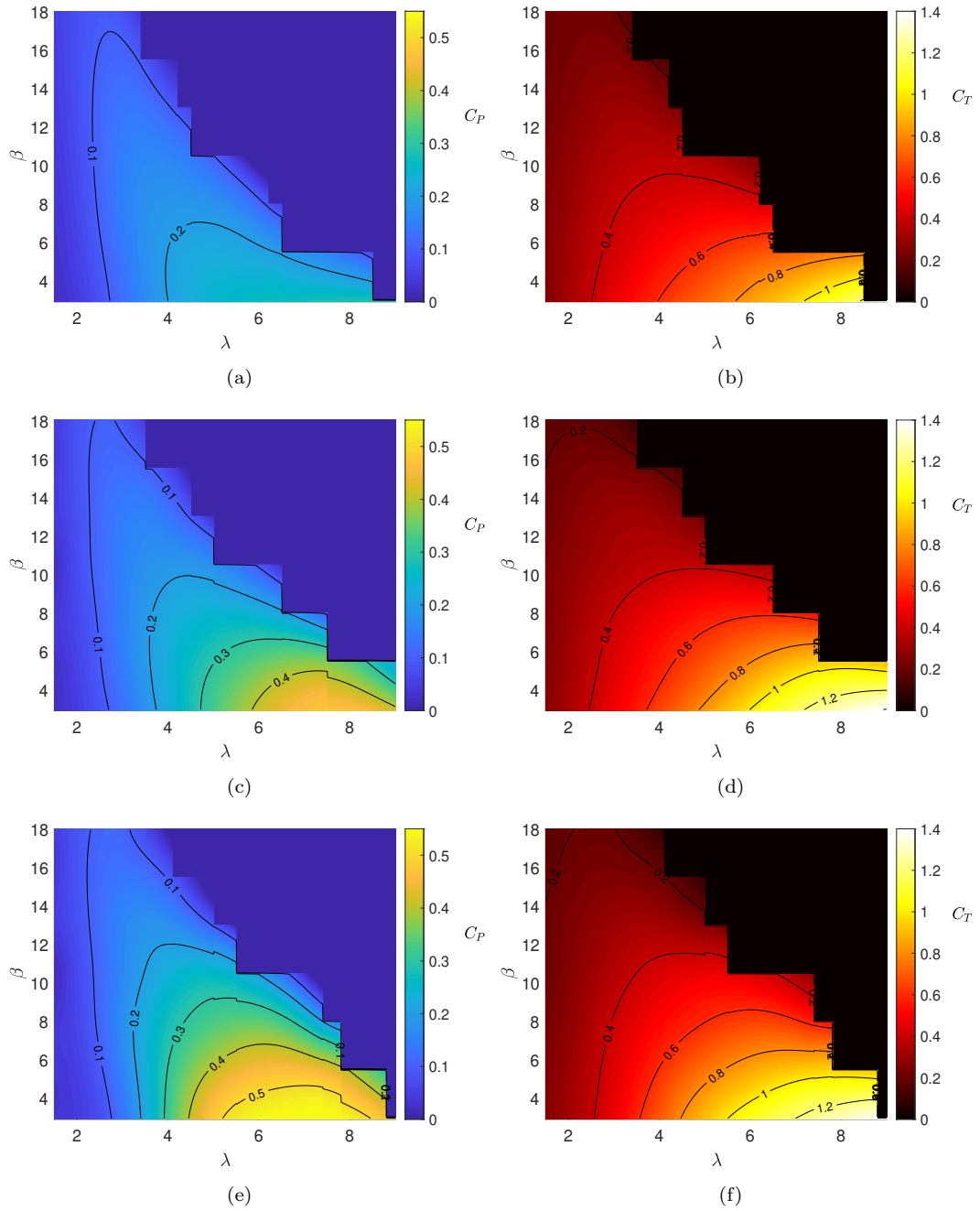

Fig. 15: C_P (left column) and C_T (right column) contour maps as a function of tip-speed ratio (λ) and blade pitch (β) in (a,b) 0.4 m/s flow, (c,d) 0.5 m/s flow, and (e,f) 0.6 m/s flow.